Available online at www.sciencedirect.com
ScienceDirect
Composites Science and Technology 68 (2008) 1250–1257
COMPOSITES SCIENCE AND TECHNOLOGY
www.elsevier.com/locate/compscitech

Analysis of damage mechanisms and associated acoustic emission in two SiC/[Si–B–C] composites exhibiting different tensile behaviours. Part I: Damage patterns and acoustic emission activity

M. Moevus, D. Rouby, N. Godin *, M. R'Mili, P. Reynaud, G. Fantozzi, G. Farizy

MATEIS, INSA-Lyon, 7 Avenue Jean Capelle, 69621 Villeurbanne, France

Received 5 July 2007; received in revised form 16 November 2007; accepted 2 December 2007
Available online 8 December 2007

Abstract

The present work deals with two SiC/[Si–B–C] composites exhibiting different mechanical behaviours under tensile testing: low strain to failure for the one, high strain to failure for the other with similar ultimate strength. In the present Part I, mechanical hysteresis loops of stress–strain curves are analysed, and detailed cracking patterns are presented and quantified for both materials. The difference between both composites is explained by different values of the interfacial shear stress. Acoustic emission activities are compared as regards to the damage accumulation scenarios. In a companion paper [Moevus M, Godin N, Rouby D, R'Mili M, Reynaud P, Fantozzi G, et al. Analyse of damage mechanisms and associated acoustic emission in two SiC/[Si–B–C] [23] composites exhibiting different tensile curves. Part II: Unsupervised acoustic emission data clustering. Comp Sci Technol, in press], the AE data will be submitted to an unsupervised clustering procedure in order to distinguish the different damage mechanisms.

Keywords: A. Ceramic matrix composites; B. Stress–strain curves; B. Matrix cracking; C. Damage mechanics; D. Acoustic emission

1. Introduction

Non-oxide ceramic matrix composites (CMCs), and more particularly SiC/SiC composites have been widely studied during the last decades [1–15]. Such fibre reinforced ceramic composites are very attractive candidates for many high-temperature structural applications, because of their excellent creep resistance, high-temperature strength and light weight. Damage tolerance is achieved through the use of low shear-strength fibre coating that deflects cracks along the interfaces [6]. Future engine applications in civil aircrafts are foreseen for such composites [7–9]. These applications require very long lifetimes under in-service conditions. The concept of functional multilayered matrix was therefore recently introduced in the new generations of SiC_f/[Si–B–C] composites in order to improve the lifetime under medium and high temperatures thanks to the formation of sealant glasses [10,11]. Various authors have studied the mechanical behavior of the SiC_f/[Si–B–C] composite and the degradation mechanisms occurring at high temperatures [12–15]. Now more information is needed at intermediate temperatures: the oxidation kinetics of the different constituents are complex, and the effect of matrix sealing on the lifetime of the composite has to be examined. The current problematic is a better comprehension of the degradation mechanisms and kinetics in order to perform reliable predictions of very long lifetimes.

The acoustic emission (AE) technique seems to be a very appropriate tool to detect in situ information about the damage occurring during mechanical testing [16]. Acoustic emission is a transient wave resulting from the sudden release of stored energy during a damage process. In composite materials, matrix cracking, fibre failure, interfacial debonding and sliding are possible sources of AE. Several studies have shown that it is possible to identify the acoustic signatures of some damage mechanisms [17–22]. The

* Corresponding author. Tel.: +33 472 438 073; fax: +33 472 438 528.
E-mail address: nathalie.godin@insa-lyon.fr (N. Godin).

0266-3538/$ - see front matter © 2007 Elsevier Ltd. All rights reserved.
doi:10.1016/j.compscitech.2007.12.001

issue of the present work (described in two companion papers) is to assess if the different damage mechanisms occurring in SiC_f/[Si–B–C] composites can be detected by the AE technique and distinguished by a statistical clustering procedure. The methodology may further be applied to static fatigue tests at intermediate temperature in order to perform lifetime predictions.

The study will focus on two SiC_f/[Si–B–C] composites exhibiting substantially different stress–strain behaviours at room temperature. The comparison between them represents an interesting opportunity to assess the AE analysis methodology. In this paper an experimental study of these two composites leads to the identification of two distinct scenarios of damage accumulation. It is shown that different mechanical behaviours lead to distinct AE activities in each composite. So it seems possible to find some link between AE and damage mechanisms. In the companion paper [23], a pattern recognition-based analysis of the AE data will be presented in order to identify the AE signatures of the main damage mechanisms.

2. Materials

The present study deals with two materials of the same family: both have a multilayered [Si–B–C] matrix reinforced with Hi–Nicalon fibres and a carbon interphase layer. The fibre preform is composed of a stacking of woven cloths in the X–Y plane. The multilayered matrix was processed by several chemical vapour infiltration steps with different compositions from the ternary [Si–B–C] system: SiC, B_4C and Si–B–C. Some macroporosity (nearly 12% volume fraction) still exists between adjacent and crossed yarns. Once the specimens are machined from the initial plate of material, an external seal-coat is processed by several chemical vapour deposition steps, which results in closing the open porosity of the tensile specimens and increasing the matrix volume fraction. The seal-coat has the same mechanical role as the matrix in the composite, it is submitted to cracking at small applied strain, whereas the fibres will fail at higher applied strain.

By this elaboration process, two composites exhibiting significant differences in the mechanical behaviour were obtained. They are noted M-E (elongation) and M-S (stiffness) (Fig. 1). The origin of such difference was not clearly identified. The cycled tensile tests presented in Fig. 1 were performed at room temperature, with a displacement rate equal to 0.2 mm/min, except during the unload–reload cycles where the rate was 2 mm/min. Both materials exhibit nearly the same initial Young's modulus (205 GPa for M-E and 225 GPa for M-S) but M-E fails after a twice larger elongation than M-S. The ultimate strength of M-S (321 MPa) is a bit higher than that of M-E (293 MPa).

Our own experimental study is based on special tensile tests described in the next section. Results of post-mortem microscopic investigation are presented to specify the differences in the damage accumulation of both materials.

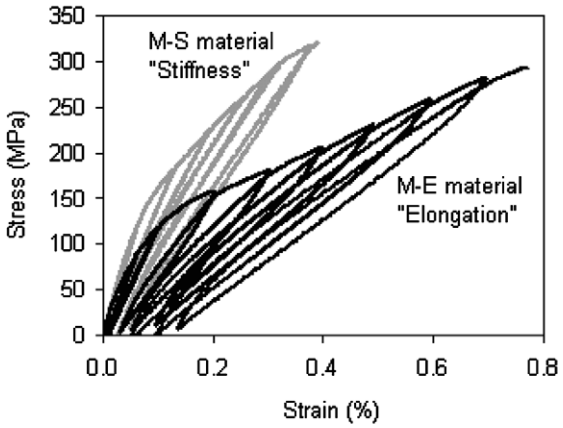

Fig. 1. Stress–strain curves by cycled tensile test. Black: M-E material; grey: M-S material.

Then the global AE activity is discussed in relation with the observations made after the tests.

3. Experimental procedure

3.1. Mechanical testing

The tests were conducted on a servohydraulic INSTRON 8502 machine at room temperature. Dog bone-shaped tensile specimens were used. Their dimensions are specified in Fig. 2a. The specimen M-E is 3.5 mm thick, whereas the M-S one is 4.5 mm thick. The fibre and matrix volume fractions before the seal-coat deposition are the same in both composites. It was decided to perform special tensile tests including a constant load-hold step which is representative of in-service conditions, followed by unload–reload cycles to characterize the influence of the preceding step on the mechanical behaviour. The applied loadings are schematised in Fig. 3. The specimens were first loaded in tension at a constant rate of 600 N/min up to the test load (O → S), which corresponds to a strain equal to 0.3%: 184 MPa for M-E and 280 MPa for M-S. The load

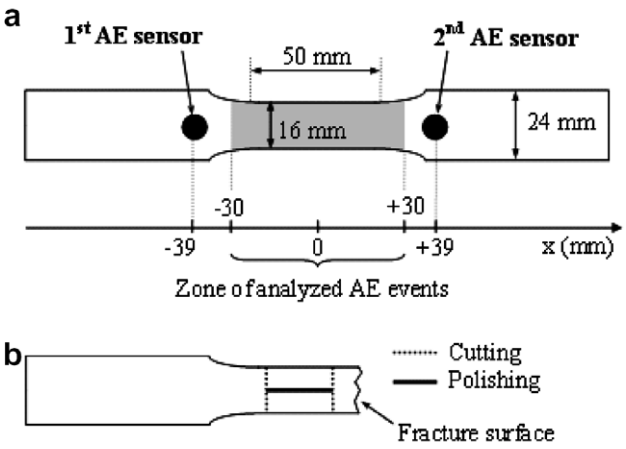

Fig. 2. Dimensions of the specimens and position of the AE sensors (a), and description of sample preparation after fracture for microscopic observations (b).

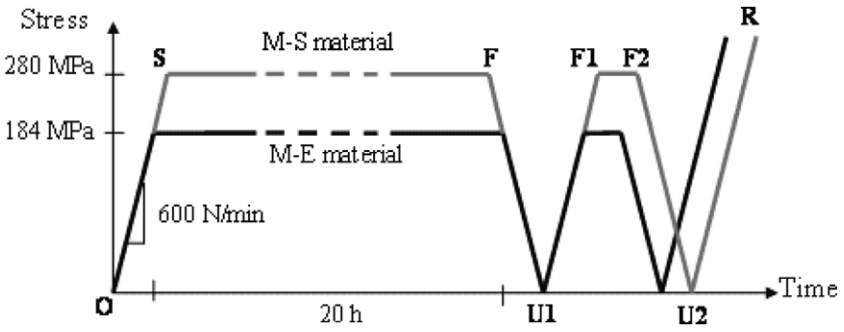

Fig. 3. Load sequences during the tensile tests monitored by AE.

was hold during 20 h (S → F). An unload–reload cycle (F → U1 → F1) was performed before unloading (F2 → U2), and it was followed by a residual tensile test up to failure (U2 → R) with the same loading rate.

3.2. Acoustic emission

AE was continuously monitored during the tensile tests by using a two-channel MISTRAS 2001 acquisition system of Physical Acoustics Corporation (PAC) with a sampling rate of 8 MHz. Pre-amplification of 40 dB and band-pass filtering of 20–1200 kHz was performed by pre-amplifiers. AE measurements were achieved by using two MICRO-80 PAC sensors. They were attached to the specimen with Teflon ribbon at the positions −39 and +39 mm, as schematized in Fig. 2a (0 mm being the centre of the gauge length). Medium viscosity vacuum grease was used as a coupling agent. A threshold of 40 dB was necessary to filter the ambient noise. The signals having a very high frequency (>900 kHz) were filtered because they may correspond to electromagnetical noise.

Before each test, the calibration of the acquisition parameters was achieved by performing a pencil lead break [24] procedure. Preliminary measurements allowed us to set up the acquisition parameters as follows for both composites: peak definition time 50 μs, hit definition time 100 μs, hit lockout time 1000 μs. The AE wave velocities have been measured in both materials before the tests by calculating the difference in time of arrival on each sensor of several lead break signals, generated at well-known positions. The initial velocity was found equal to 10,000 m/s in both composites. A smaller value has been measured on damaged composites, suggesting that the velocity decreases as Young's modulus decreases during mechanical testing. To perform reliable estimations of the sources' positions we have to take into account this variation as a function of strain. The velocity of an extensional wave in a thin plate is proportional with the square root of the elastic modulus E of the material. So as proposed by Morscher [25,26], the initial modulus during unloading $E(\varepsilon)$ was measured from the cycled tensile tests presented in Fig. 1. The velocity $Ce(\varepsilon)$ was then determined by: $Ce(\varepsilon)/Ce_0 = \sqrt{E(\varepsilon)/E_0}$ where Ce_0 and E_0 are, respectively, the velocity and the elastic modulus in the undamaged state. At the end of the test, the velocity was found to be equal to 6480 m/s, in M-E, instead of 10,000 m/s in the undamaged state. The decrease in wave velocity is thus not negligible. The linear location of each AE source has been calculated by using the difference in time of arrival on each sensor and the previously described strain-dependant velocity $Ce(\varepsilon)$, in a location algorithm programmed in MATLAB. Finally, we kept only the signals coming from the central part of the specimen (between −30 and +30 mm, Fig. 2a).

3.3. Microscopic observations

Optical microscopy and scanning electron microscopy (SEM) were used to observe and characterize the damage state of the samples. The specimens were cut after the mechanical tests according to the Fig. 2b. The fracture surfaces were observed using a JEOL 840A-LGS SEM system in order to measure the mean pull-out length of the fibres. A parallel to load-surface in the core of the sample was cut and polished. Murakami's etching was used to reveal the cracks before the observations by optical microscopy. In this way the cracks could be located and counted.

4. Results

4.1. Preliminary discussion on the mechanical behaviours

Before the presentation of the results, it is interesting to analyse the cycled tensile tests presented in Fig. 1. The elongation of M-E is twice higher than that of M-S and the hysteresis loops are more open in M-E, although the constituents and proportion of them are nearly the same (same initial elastic modulus). Wide hysteresis loops in M-E suggest that sliding at the fibre–matrix interface widely occurs in this composite, leading to some energy dissipation during the unload–reload cycles. On the contrary, M-S hysteresis loops are very little open, so interfacial sliding appears to be limited in M-S. The difference between both composites could be explained by a weaker interfacial shear stress in M-E than in M-S.

Reynaud et al. [27,28] have shown that for a unidirectional composite, the results of the analytical calculation

of the mechanical hysteresis ($\Delta W/W_e$) as a function of the interfacial shear stress (τ) are

$$\text{if } \tau/\tau^* \geqslant 1, \quad \frac{\Delta W}{W_e} = \frac{\alpha}{3(\alpha/2 + \tau/\tau^*)} \tag{1}$$

$$\text{if } \tau/\tau^* \leqslant 1, \quad \frac{\Delta W}{W_e} = \alpha(\tau/\tau^*)\frac{1 - \frac{2}{3}\tau/\tau^*}{1 + \alpha(1 - \frac{1}{2}\tau/\tau^*)} \tag{2}$$

where $W_e = \frac{1}{2}\sigma^2/\langle E\rangle$, $\alpha = E_m V_m/E_f V_f$, and $\tau^* = \alpha r E_f \sigma/(2dE_c)$ with ΔW is the stress–strain loop area, W_e is elastic strain energy, σ is the maximum applied stress, $\langle E\rangle$ is the mean elastic modulus of the hysteresis loop, r is the radius of the fibres, d is the mean crack spacing, E_f, V_f, E_m, and V_m is Young's modulus and volume fractions of the fibres and the matrix, respectively, and $E_c = E_f V_f + E_m V_m$ is Young's modulus of the composite. The parameter τ^* corresponds to the limit value of interfacial shear stress between a local and a total sliding of the fibres. This limit also corresponds to the case of matrix cracking saturation. The theoretical calculation of $\Delta W/W_e$ as a function of τ/τ^* leads to a unique curve (Fig. 4) only dependent on the constituent properties and proportions. When τ/τ^* increases, the hysteresis $\Delta W/W_e$ increases up to a maximum value at $\tau/\tau^* = 0.87$, following a parabolic law up to $\tau/\tau^* = 1$, and then hyperbolically decreases. During a cycled tensile test on a unidirectional composite, the applied stress σ increases from a cycle to the other, and matrix cracks appear leading to a decreasing crack spacing value d. So as stress increases, d decreases and $\tau^* = \alpha r E_f \sigma/(2dE_c)$ increases. The interfacial shear stress τ can be considered as constant or little decreasing during the test since very few cycles are applied. Therefore τ/τ^* continuously decreases during a cycled tensile test. For the running point M1 (Fig. 4) with $\tau/\tau^* > 1$ and near the maximum of $\Delta W/W_e$, the hysteresis loop area is expected to increase as stress increases, before reaching a maximum width and then decreasing. If τ/τ^* is very high (running point M2 on Fig. 4), the maximum will not be reached during the cycled tensile test, and the increase in hysteresis loop area will be smaller than for M1.

The experimental measurements of the mechanical hysteresis as a function of applied stress are presented in Fig. 5

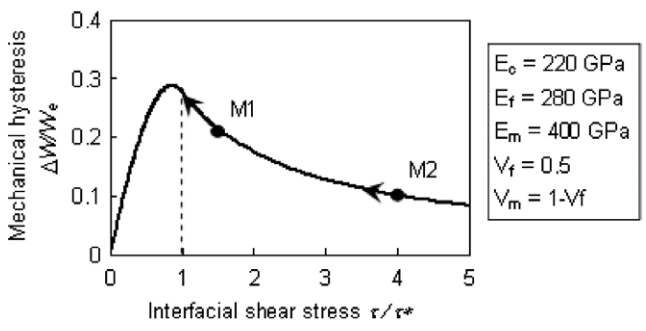

Fig. 4. Theoretical effect of the interfacial shear stress (τ) on the mechanical hysteresis (ΔW) in a unidirectional composite with a fibre volume fraction of 50% (W_e: elastic strain energy; τ^*: limit value of τ between local and total sliding of the fibres).

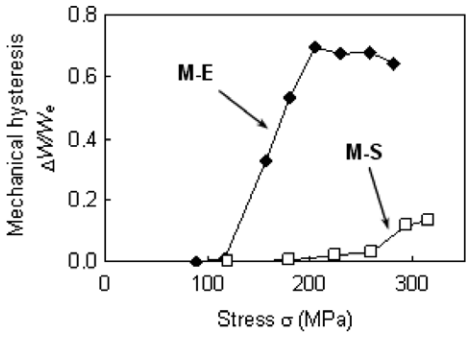

Fig. 5. Mechanical hysteresis measures as a function of applied stress during cycled tensile tests on M-E and M-S composites.

for both materials. The numerical values of $\Delta W/W_e$ cannot be directly compared with the theoretical curve shown in Fig. 4 because it was calculated for a unidirectional composite with no porosity. However the evolution of $\Delta W/W_e$ during cycled tensile tests on M-E and M-S are comparable, respectively, with the M1-like and M2-like behaviours. So the initial value of τ/τ^* is bigger in M-S than in M-E, leading to very different evolutions of the mechanical hysteresis. Matrix cracking saturation has been achieved in M-E at the end of the test since the mechanical hysteresis reaches a maximum. The difference in τ/τ^* can be explained whether by a higher τ^* value in M-E (linked with a smaller crack spacing value d), or by a higher τ value in M-S. The microscopic observations will help us to conclude.

4.2. Mechanical results

During the special tests described in Section 3, both composites exhibit similar behaviours as those presented in Fig. 1: larger strain to failure for M-E with more open hysteresis loops. Small differences exist in the case of M-S composite between the cycled tensile test and the special one including a load-hold sequence (Fig. 6): the residual

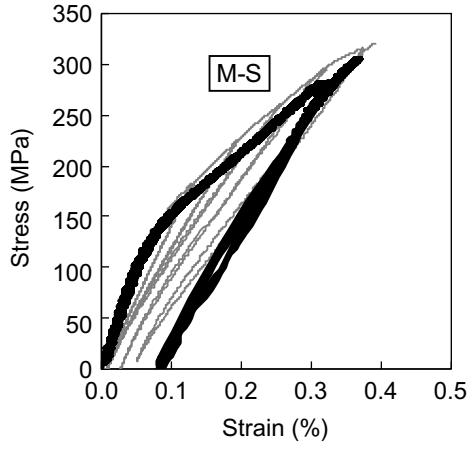

Fig. 6. Comparison of the stress–strain curves of M-S composite obtained during a cycled tensile test (grey) and during a special tensile test including a static load-hold sequence (black).

strain in M-S after unloading is equal to 0.08%, whereas it was equal to 0.03% for similar unload–reload cycle during the cycled tensile test. This difference may result from some degradation during the load-hold step before unloading. In M-E the load-hold step had no visible influence on the mechanical behaviour.

4.3. Microscopy

Micrographs of the fracture surfaces (Fig. 7) revealed some differences between the studied composites. The pull-out lengths of approximately 300 fibres were measured for each specimen. Mean values and standard deviations (in brackets) are given in Table 1. The mean pull-out length appeared to be six times higher in M-E than in M-S. Another difference between the fracture surfaces is that the yarn's surface is planar and perpendicular to load in M-E, whereas it is clearly non-planar in M-S. This suggests that the fracture of yarns result from the propagation of a single matrix crack in M-E, whereas the coalescence of several matrix cracks has more likely caused the fracture of yarns in M-S.

The observations of polished surfaces give useful information about the crack network in each material. Location and nature of cracks are summarized in Fig. 8, and mean crack spacing distances are given in Table 1. In both composites we principally observed cracks perpendicular to load: in inter-yarn matrix layers (C1-cracks, initiated either at the external seal-coat or at the macropores inside the composite), in transverse yarns (C2), and finally inside the axial yarns (C3). C2-cracks run inside the transverse yarns through fibre–matrix interfaces. Therefore this type of cracking may be a step-by-step mechanism. In the core of M-S, an additional cracking was clearly observed in one of the matrix layers (C5, Fig. 8b).

Table 1
Mean values (standard deviation in brackets) of the pull-out lengths and crack spacing values of M-E and M-S composites

	Pull-out length	Inter-yarn matrix crack spacing (C1)	Intra-yarn matrix crack spacing (C3)	Crack spacing (C5) in a particular layer
M-E (μm)	300 (250)	840 (450)	330 (150)	Same as C1
M-S (μm)	55 (50)	420 (260)	65 (50)	180 (120)

Concerning more precisely the composite M-E (Fig. 8a), the cracks are fairly open. Some evidence of debonding can be seen between fibres and matrix in the transverse yarns (C2-cracks) and also between some seal-coat and matrix layers. Some debonding (C4) associated with C3-cracks is probably occurring in the axial yarns but it was not easily observed. The large extraction of the fibres confirms this assumption. This would explain the larger strain to failure of this material. Moreover, cracks are commonly observed that run from the seal-coat through several axial and transverse yarns.

In the case of the composite M-S (Fig. 8b), the same cracks have been observed but they are very few open and very close together. This suggests that interfacial debonding (C4) and load transfer between fibres and matrix acts on very short distances, allowing a dense

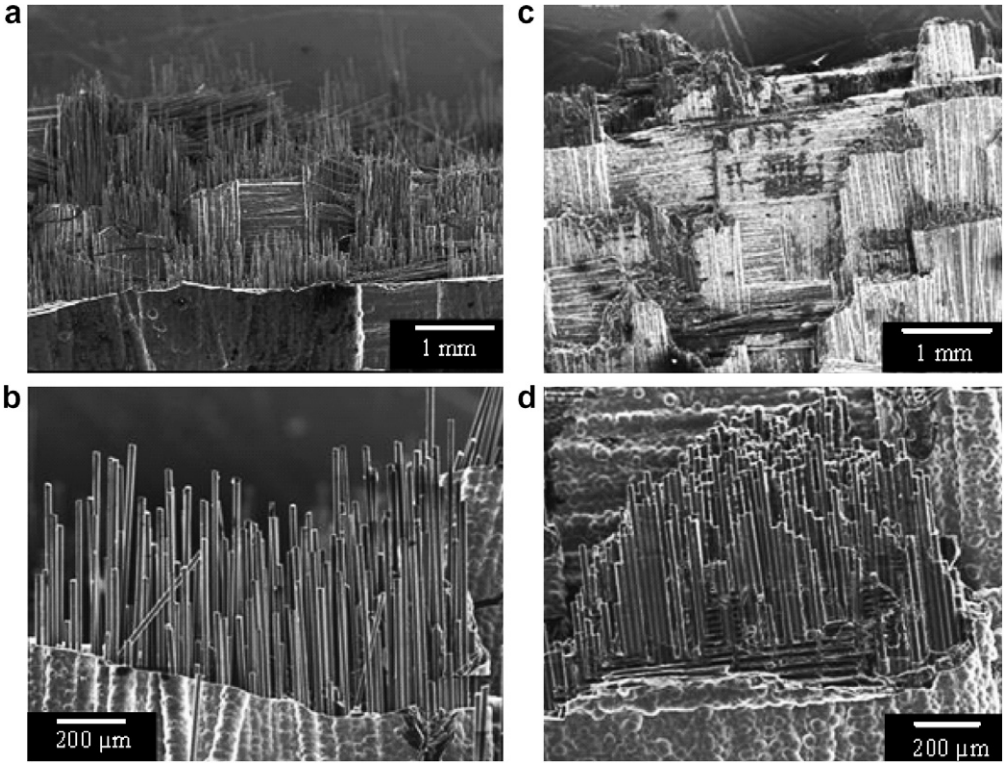

Fig. 7. Micrographs showing the fracture surface of M-E material (left: a, b) and M-S material (right: c, d). The pull-out lengths are very short in M-S.

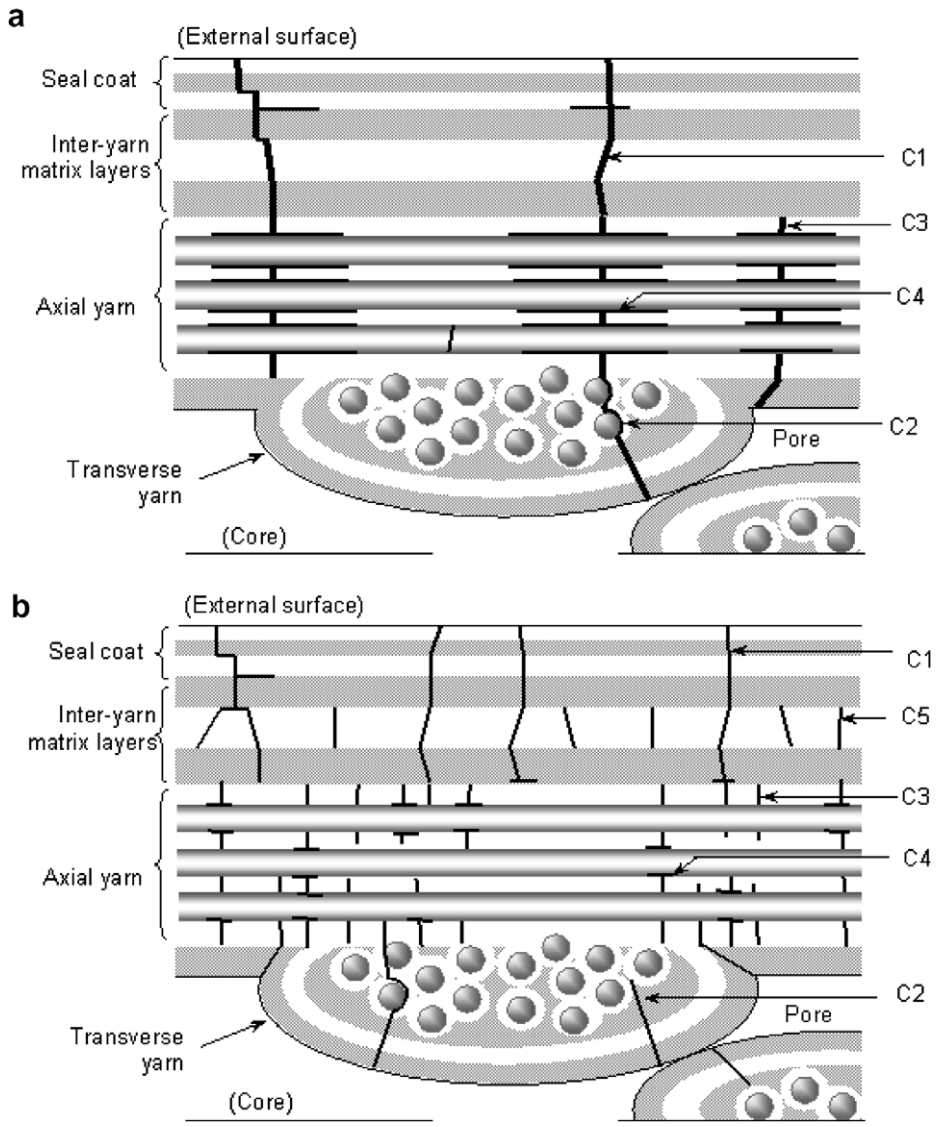

Fig. 8. Picture summarizing the different types of cracks observed after failure (a) in the M-E composite and (b) in the M-S one.

matrix cracking. This is in agreement with small strain to failure and short pull-out lengths. In this composite there is no continuity between C1-cracks and C2-cracks. C3-cracks do not cross the whole cross-section of the axial yarn, leading to a non-planar final fracture surface of the matrix (Fig. 7d). Moreover an additional mechanism is observed in this composite (dense C5-cracking in a particular matrix layer) which is also an illustration of strong interfaces between these layers (see Table 1).

In M-S, it was observed that the cracks are not regularly distributed along the axial yarns. In some zones the crack network is very dense (20 μm crack spacing), and in other zones the distances between cracks were very large (nearly 100–200 μm). So it seems that the saturation of matrix cracking was not obtained in M-S.

As a result, it has been observed that the mean crack spacing in the axial yarns (C3) is more than five times higher in M-E than in M-S. The limit value τ^* in M-S is thus five times higher than τ^* in M-E for the same applied stress. It has been emphasized in the preceding section that the ratio τ/τ^* has to be higher in M-S than in M-E. Therefore M-S-interfacial shear stress τ has to be much higher than M-E-shear stress to compensate the higher τ^* value in M-S. So M-S exhibits a stronger fibre–matrix interface than M-E, which explains the short pull-out lengths, dense matrix cracking and small crack opening observed in that material. The mean crack spacing measurements in M-E suggest that matrix cracking saturation has been achieved in this material, because the crack spacing is quite regular. This is not the case in M-S, where the standard deviation of crack spacing measurements is very high in comparison with the mean crack spacing value. This suggests that matrix cracking saturation was not achieved in this material, as it was expected in Section 4.1. Finally an additional cracking has been observed in a particular matrix layer in M-S, which was not observed in M-E.

4.4. AE activity

The observations of damage suggest that the AE should be different in M-E and in M-S: more AE sources are expected in M-S since more cracks have been counted, and some acoustic activity has to be recorded during the unload–reload cycles as interfacial sliding occurs in M-E (wide hysteresis loops). A significant activity is expected in M-S during the load-hold sequence since noticeable influence of this particular step on the stress–strain curve has been pointed out (Section 4.2).

The AE activity is plotted as a function of strain in Fig. 9 for both composites. The acoustic activity is defined here as the cumulative number of AE events. At the end of the test, three times more AE events are recorded in M-S than in M-E. This is in agreement with more cracks in that composite because of a higher interfacial shear stress. According to the testing schedule (Fig. 3), the AE curves in Fig. 9 exhibit first the initial loading up to a strain equal to 0.3%. In both materials the main AE activity appears at the beginning of non-linearity (0.03% strain). During this initial loading step, M-S appears twice more emissive than M-E, suggesting that more matrix cracks are created. Then during the hold sequence under constant load, the difference between both composites is exacerbated: the recorded events are eight times more in M-S than in M-E. For more precise observation, the activity during this step is plotted in Fig. 10a. Under constant load, interfacial debonding is expected to progress both in transverse (C2) and axial yarns (C4). The progression of C2-cracks leads to overloading of the axial yarns, and consequently to C3-matrix cracking and possibly fibre failures. The higher AE activity of M-S is globally due to its higher interfacial shear stress (smaller debonding length allowing more matrix cracks), but may be exacerbated during the load-hold step by the higher stress level, much closer to the ultimate strength than in the case of M-E. So the composite M-S appears more unstable during this hold sequence. The high activity of M-S during the hold sequence can explain the higher permanent strain observed during the special tensile test than during the cycled tensile test (Fig. 6): more damage occurred before unloading because of the 20 h load-hold in the special tensile test.

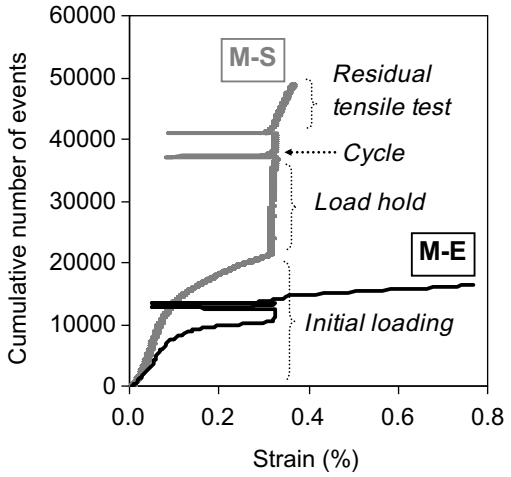

Fig. 9. AE activity of M-E (black) and M-S (grey) composites.

The hold step is followed by unload–reload cycles with not much acoustic emission. The detail of the first cycle (F → U1 → F1) is given in Fig. 10b. The composite M-E appears more active in terms of AE than M-S during unloading as it was expected: some signals have been recorded at the end of unload as interfacial sliding occurs, favoured by a weak interface and a large debonding length. Then, during reload up to the previously applied stress, some AE activity is recorded in both materials, and preferentially in M-S. So these composites exhibit a Felicity effect, and damage occurs before reaching the previously applied stress. This is probably due to some load redistribution during unload–reload cycles.

After that, the material is loaded up to failure. M-S appears more emissive again than M-E during this ultimate sequence. The last events in M-E lead to large increments of strain: with nearly 2000 events during the residual test, the strain is twice higher than that reached after initial loading with nearly 12,000 events.

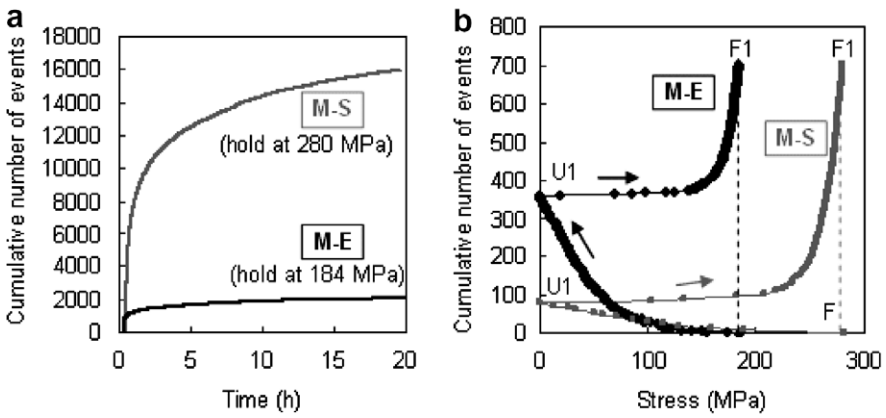

Fig. 10. Cumulative number of events (a) during load-hold sequence S → F, and (b) during unload–reload cycle F → U1 → F1.

5. Conclusion

The differences between two composites exhibiting different behaviours have been presented and analyzed by comparing the mechanical hysteresis, and by describing the damage state after mechanical testing. It was concluded that the difference between the studied composites was due to manifestly different interfacial shear stress values. The AE recorded during the tests has been carefully filtered in order to keep only the signals created by damage mechanisms. As a result, the global AE activity is in good agreement with the observed damage mechanisms: more signals in M-S because of a larger number of cracks, more AE during the load-hold in M-S, and more AE during unload in M-E because of sliding mechanisms. The AE data will now be submitted to a pattern recognition procedure in order to distinguish the different occurring damage mechanisms. This further analysis is detailed in a companion paper [23].

Acknowledgements

The authors gratefully acknowledge Snecma Propulsion Solide, CNRS and DGA for supporting this work in the frame of the CPR: 'Modélisation, extrapolation, validation de la durée de vie des CMC'.

References

[1] Fantozzi G, Reynaud P, Rouby D. Thermomechanical behaviour of long fibres ceramic–ceramic composites. Silic Ind 2002;66:109–19.
[2] Reynaud P, Dalmaz A, Tallaron C, Rouby D, Fantozzi G. Apparent stiffening of ceramic–matrix composites induced by cyclic fatigue. J Eur Ceram Soc 1998;18(13):1827–33.
[3] Morales-Rodríguez A, Moevus M, Reynaud P, Fantozzi G. Strength enhancement of 2D-SiC_f/SiC composites after static fatigue at room temperature. J Eur Ceram Soc 2007;27(11):3301–5.
[4] Evans AG. Perspective on the development of high-toughness ceramics. J Am Ceram Soc 1990;73(2):187–206.
[5] Evans AG, Zok FW. Review: the physics and mechanics of fibre-reinforced brittle matrix composites. J Mater Sci 1994;29:3857–96.
[6] Naslain R. The design of the fibre–matrix interfacial zone in ceramic matrix composites. Compos Part A 1998;29A:1145–55.
[7] Naslain R. Design, preparation and properties of non-oxide CMCs for application in engines and nuclear reactors: an overview. Comp Sci Technol 2004;64:155–70.
[8] Naslain R, Christin F. SiC–matrix composite materials for advanced jet engines. MRS Bull 2003;28(9):654–8.
[9] Ohnabe H, Masaki S, Onozuka M, Miyahara K, Sasa T. Potential applications of ceramic matrix composites to aero-engine components. Compos Part A 1999;30:489–96.
[10] Lamouroux F, Bertrand S, Pailler R, Naslain R, Cataldi M. Oxidation-resistant carbon–fiber-reinforced ceramic–matrix composites. Comp Sci Technol 1999;59:1073–95.
[11] Quémard L, Rebillat F, Guette A, Tawil H, Louchet-Pouillerie C. Self-healing mechanisms of a SiC fiber reinforced multi-layered ceramic matrix composite in high pressure steam environments. J Eur Ceram Soc 2007;27:2085–94.
[12] Forio P, Lamon J. Fatigue behavior at high temperatures in air of a 2D SiC/SiBC composite with a self-sealing multilayered matrix. In N.P. Bansal, J.P. Singh, H.T. Lin, editors. Ceram Transactions, vol. 128. Westerville:American Ceramic Society;2001. pp. 127-141.
[13] Carrère N, Lamon J. Creep behaviour of a SiC/Si–B–C composite with a self-healing multilayered matrix. J Eur Ceram Soc 2003;23:1105–14.
[14] Farizy G, Chermant JL, Vicens J, Sangleboeuf JC. Understanding of the behaviour and the influence of oxidation during creep of SiC–SiBC composites in air. Adv Eng Mater 2005;7(6):529–34.
[15] Reynaud P, Rouby D, Fantozzi G. Cyclic fatigue behaviour at high temperature of a self-healing ceramic matrix composite. Ann Chim Sci Matér 2005;30(6):649–56.
[16] Beattie AG. Acoustic emission, principles and instrumentation. J Acoust Emission 1983;2(1/2):95–128.
[17] Anastassopoulos AA, Philippidis TP. Clustering methodology for the evaluation of AE from composites. J Acoust Emission 1995;13(1/2):11–22.
[18] Kostopoulos V, Loutas TH, Kontsos A, Sotiriadis G, Pappas YZ. On the identification of the failure mechanisms in oxide/oxide composites using acoustic emission. NDT&E Int 2003;36:571–80.
[19] Pappas YZ, Kontsos A, Loutas TH, Kostopoulos V. On the characterization of continuous fibres fracture by quantifying acoustic emission and acousto-ultrasonics waveforms. NDT&E Int 2004;37:389–401.
[20] Kostopoulos V, Loutas T, Dassios K. Fracture behavior and damage mechanisms identification of SiC/glass ceramic composites using AE monitoring. Comp Sci Technol 2007;67:1740–6.
[21] Huguet S, Godin N, Gaertner R, Salmon L, Villard D. Use of acoustic emission to identify damage modes in glass fibre reinforced polyester. Comp Sci Technol 2002;62:1433–44.
[22] Godin N, Huguet S, Gaertner R. Integration of the Kohonen's self-organising map and k-means algorithm for the segmentation of the AE data collected during tensile tests on cross-ply composites. NDT&E Int 2005;38(4):299–309.
[23] Moevus M, Godin N, Rouby D, R'Mili M, Reynaud P, Fantozzi G, et al. Analysis of damage mechanisms and associated acoustic emission in two SiC/[Si–B–C] composites exhibiting different tensile curves. Part II: unsupervised acoustic emission data clustering. Comp Sci Technol 2008;68(6):1258–65.
[24] Nielsen A. Acoustic emission source based on pencil lead breaking. The Danish Welding Institute Publication; 1980.
[25] Morscher GN. Stress dependent matrix cracking in 2D woven SiC–fibre reinforced melt-infiltrated SiC matrix composites. Comp Sci Technol 2004;64:1311–9.
[26] Morscher GN. The velocity and attenuation of acoustic emission waves in SiC/SiC composites loaded in tension. Comp Sci Technol 2002;62:1171–80.
[27] Reynaud P. Etude du comportement en fatigue des matériaux composites à matrice céramique suivi par émission acoustique. Thèse de doctorat, INSA-Lyon; 1992.
[28] Reynaud P, Rouby D, Fantozzi G. Effects of temperature and of oxidation on the interfacial shear stress between fibres and matrix in ceramic–matrix composites. Acta Mater 1998;46(7):2461–9.